Study on 3D printing technology and mechanical properties of a nano-enhanced composite hydrogel bio-ink

Weitao Wu ✉

School of Mechanical Engineering, Liaoning Equipment Manufacture College of Vocational Technology, Shenyang 110161, People's Republic of China
✉ *E-mail: wuwei3201@163.com*

Published in Micro & Nano Letters; Received on 19th November 2019; Revised on 30th July 2020; Accepted on 18th August 2020

Traditional bio-inks are mostly limited in application due to their low-mechanical strength or complex cross-linking curing methods. In this study, a nanocomposite hydrogel bio-ink [gelatin–alginate–montmorillonite (GT–AT–MMT)] for 3D bioprinting is designed based on the thermo-sensitive properties of GT, the advantages of ionic crosslinking of sodium AT, and the shear thinning and toughening mechanism of nano-MMT. The 3D printing of the bio-ink with variable AT content is optimised, and the tensile, compressive, and creep properties of the 3D printed structure are studied. Results show that GT–AT–MMT bio-ink has good printability, and its mechanical properties are enhanced with increased AT content. The tensile modulus of the GT–4% AT–MMT sample can reach 0.533 MPa, which has a minimum creep deformation of 0.311 mm under the same load condition. Therefore, GT–AT–MMT bio-ink provides a new possibility for the development of 3D bioprinting, which will offer many opportunities in fields such as tissue engineering, drug delivery, and regeneration medicine.

1. Introduction: The 3D bioprinting mainly uses bio-inks to build complex 3D tissue structures, creating various implants and scaffolds for regenerative medicine and tissue engineering [1, 2]. A 3D scaffold must have controllable pore size, high porosity, and good pore connectivity [3–5] because it needs to simulate the tissue extracellular matrix [6, 7]; thus proper choice of bio-inks [8] and parameter optimisation of printing [2, 9] are two focuses of 3D bioprinting. In previous studies, natural polymers (collagen [10], silk fibroin [11], and nanocellulose [12, 13]) and synthetic polymers (polyvinyl alcohol [14] and polyethylene glycol [15]) hydrogel bio-inks were successfully applied to 3D bioprinting and made some progress.

Gelatin (GT) is a fibrin obtained from the triple helix structure of collagen and is characterised by degradability, good biocompatibility, low-antigenic characteristics, and high cell-adhesion ability [16, 17]. More importantly, GT has sensitive thermal property and can form a gel at low temperatures. Therefore, GT is widely used as a bio-ink material for 3D printing. However, pure GT bio-ink has low-mechanical strength and rapid degradation rate; thus it is usually mixed with other natural biomaterials.

Sodium alginate (AT) is a natural anionic polysaccharide, which has the advantages of being low priced, non-toxic, and easy to gel under mild conditions. It is widely used in medicine, food, chemistry, biology, and other fields [18]. However, AT has disadvantages such as few cell attachment sites, poor degradability, and polymerisation shrinkage after crosslinking, which cannot meet the expected performance requirements when used alone [19]. In addition, it is not easy to extrude from the printing nozzle because the viscosity of sodium AT bio-ink increases significantly with the increase in its concentration. Therefore, some nanomaterials must be added to AT-based bio-inks to change the shear-thinning ability [20–22].

Montmorillonite (MMT) is a layered nanosilicate composed of disk-like nanoparticles with a positively charged edge and a negatively charged surface. The uneven distribution of the whole disk structure leads to the formation of a well-structured fluid due to the electrostatic interaction between nanoparticles [23]; thus MMT is widely used as a modifier and additive for rheology, and recent studies showed that it can significantly affect the flow behaviour and mechanical properties of a hydrogel matrix [24, 25].

In this study, a mixture of GT, AT, and MMT was used as a nanocomposite bio-ink for 3D printing to explore the 3D printability of GT–AT–MMT bio-ink and the parameter optimisation of the 3D printing. In addition, the mechanical properties of the 3D printing structure of GT–AT–MMT bio-ink with variable AT concentrations were studied to provide a new possibility for the development of 3D bioprinting in the field of cartilage tissue engineering and regenerative medicine.

2. Experimental section

2.1. Experimental materials: GT (microbiology grade, bloom strength ~250 g) was purchased from MACKLIN Reagent Company. AT (viscosity 200 ± 20 MPa·s of pure AT), MMT (white powder, nanometre particle size), and anhydrous calcium chloride (white powder, non-toxic, and non-corrosive) were obtained from Aladdin Reagent Company.

2.2. Preparation of GT–AT–MMT bio-inks: A certain amount of GT, AT, and MMT (Fig. 1*a*) was weighed and poured into beakers. A corresponding proportion of deionised water was added (Table 1), then stirred with a glass rod, and covered with plastic wrap at room temperature for 2 h. Subsequently, the beakers were placed in a 50°C electronic water bath pot to stir magnetically for 12 h. Finally, the homogeneous hydrogel precursors were injected into 3D printing cartridges, underwent ultrasonic oscillation for 5 h to remove bubbles, and placed in a 4°C refrigerator for use.

2.3. Process optimisation of 3D printing GT–AT–MMT: The control variable method was used in this experiment. For bio-inks with different AT contents, the preheating temperature of the cartridge was similarly set to 50°C, the inner diameter of the nozzle was similarly set to 0.30 mm, and the uniform printing speed of 3 mm/s was set to explore the optimum printing pressure for GT–AT–MMT bio-inks with different AT contents. The extruding drop test and experiment of 3D printing checkerboard grid structure (edge length 15 mm × 15 mm, filament spacing 1 mm) were designed. The ratio (F_{ma}) between the actual pore area and the theoretical pore area was calculated to determine optimum pressure by observing the shape of extruded hydrogel filaments

doi: 10.1049/mnl.2019.0712

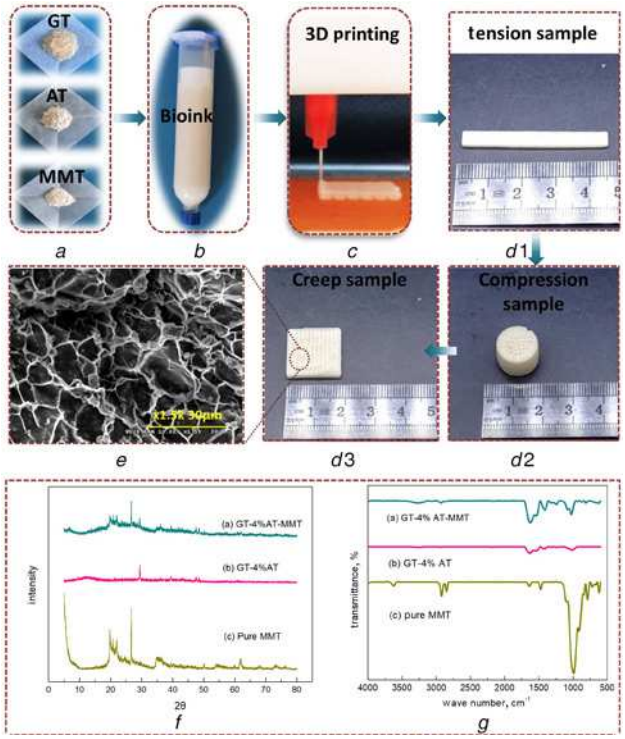

Fig. 1 *Preparation of GT–AT–MMT bio-inks and 3D printed samples*
a Raw materials of bio-ink
b GT–AT–MMT bio-ink cartridge for 3D printing
c 3D printing of GT–AT–MMT bio-ink
d_1–d_3 3D printed tension sample, compression sample, and creep sample
e SEM of 3D printed GT–AT–MMT
f XRD patterns of 3D printed GT–AT–MMT
g FTIR patterns of 3D printed GT–AT–MMT

Table 1 Composition of GT–AT–MMT composite hydrogel bio-inks

Number	GT (w/v), %	AT (w/v), %	MMT (w/v), %	Deionised water (w/v), %
GT–2% AT–MMT	10	2	6	82
GT–3% AT–MMT	10	3	6	81
GT–4% AT–MMT	10	4	6	80

directly and observing the 3D printed structure with a high-speed microscope camera

$$F_{ma} = \frac{A_e}{A_t},$$

where A_e is the actual pore area and A_t is the theoretical pore area.

2.4. Tension test: An electronic universal testing machine (model: WDW-2) was used to examine the 3D printed GT–AT–MMT samples (rectangular 50 mm × 5 mm × 2 mm), and the strain rate was 2 mm/min. The samples were immersed in deionised water to swell fully before the experiment.

2.5. Compression test: An electronic universal testing machine (model: WDW-2) was used to examine the 3D printed GT–AT–MMT samples (cylindrical, diameter 15 mm × height 10 mm), the compression rate was 10 mm/min, and compression deformation was 25% of sample height. The samples were immersed in deionised water to swell fully before the experiment.

2.6. Creep test: The creep behaviour of 3D printed GT–AT–MMT samples (square 15 mm × 15 mm × 2 mm) was tested using a UMT-II testing machine. The test adopted a cylindrical indenter of Φ 8 mm, a preloading force of 5 N, a time of 5 s, a formal load of 10 N, and a duration of 1 h.

2.7. Microscopic characterisation: SEM (Quanta250, FEI, USA) was used to observe the microstructure of the 3D printed GT–AT–MMT samples. XRD (Bruker D8 ADVANCE, Germany) and Fourier transform infrared spectroscopy (FTIR, Bruker VTRTEX 80V, Germany) were adopted for phase analysis.

3. Results and analysis

3.1. 3D printing samples with GT–AT–MMT bio-inks: The prepared GT–AT–MMT hydrogel bio-ink cartridge (Fig. 1*b*) was loaded into the 3D printer, the temperature of the bio-ink cartridge was set to 50°C, and the temperature of the printing platform was set to 4°C. According to the pre-designed stereolithography (STL) format models, a rectangular sample (50 mm × 5 mm × 2 mm) was printed for the tensile test (Fig. 1*d*1) with a 90° superposition between layers (Fig. 1*c*), a cylindrical sample (diameter 15 mm × height 10 mm) was printed for the compression test (Fig. 1*d*2), and a square sample (15 mm × 15 mm × 2 mm) was printed for the creep test (Fig. 1*d*3). The printed samples were then placed at 4°C in a refrigerator for 5 h to achieve preliminary shaping of the printed structure by low-temperature curing. Finally, the samples were immersed in $CaCl_2$ solution of 3% (w/v) for cross-linking. After 12 h, the samples were taken out and cleaned with deionised water for six times (water was changed every 6 h) to remove excess $CaCl_2$. SEM (Fig. 1*e*) exhibits that the 3D printed GT–AT–MMT hydrogel has a loose, porous network structure with interposed nanoparticles. XRD (Fig. 1*f*) and FTIR patterns (Fig. 1*g*) show that the addition of

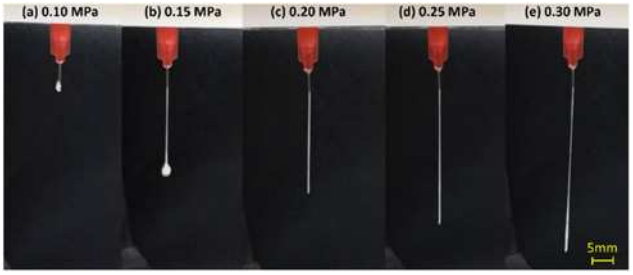

Fig. 2 *Dropping filament morphologies of GT–2% AT–MMT bio-ink under variable pressure parameters of 0.10, 0.15, 0.20, 0.25, and 0.30 MPa*

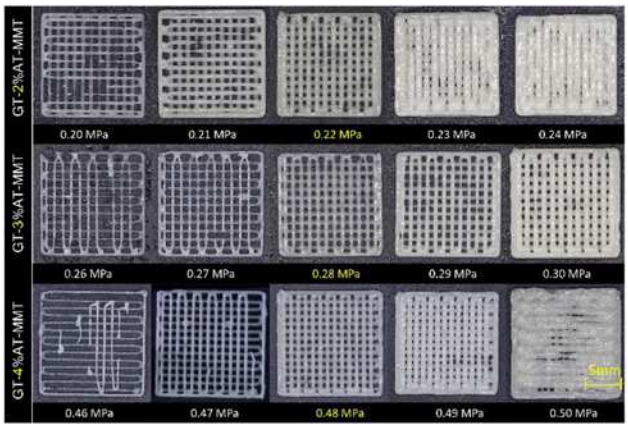

Fig. 3 *Sample morphologies printed with GT–AT–MMT bio-inks of variable concentrations under predetermined pressures*

Table 2 Optimised pressure range of 3D printing variable GT–AT–MMT bio-inks

Bio-inks	GT–2% AT–MMT	GT–3% AT–MMT	GT–4% AT–MMT
optimised pressure range	0.20–0.25 MPa	0.26–0.30 MPa	0.45–0.50 MPa

MMT promotes the crystallisation degree of GT–AT–MMT, and a hydrogen bond interaction is formed between MMT, GT, and AT, thus enhancing the intermolecular binding force and the crosslinking degree of the 3D printed GT–AT–MMT hydrogel.

3.2. Pressure optimisation by the extruding drop test: The range of the appropriate pressure can be approximately optimised by visually observing the morphology of extruded filaments in 3D printing. Taking GT–2% AT–MMT bio-ink as an example, Fig. 2 shows the morphology of dropping filament under different pressure parameters. The extrusion pressure of 0.10 MPa is very small, resulting in a very slow extrusion rate of the bio-ink, and the shear thinning effect is not evident. A small amount of bio-ink slowly reaches the nozzle, and the viscosity of the bio-ink increases significantly due to the temperature fall after extrusion, thus blocking the nozzle. The extrusion pressure of 0.15 MPa is also insufficient. Although the filament can be extruded, the bio-ink agglomerates first at the nozzle due to the slow speed and then drops with gravity. Extrusion pressures of 0.20 and 0.25 MPa show an ideal situation with a moderate extrusion rate and a good filament continuity, which can form a uniform filament. When the pressure is 0.30 MPa, the extrusion rate is so high that the bio-ink material is extruded in a manner similar to spraying, presenting an uneven form of an upper fine and lower coarse. The dripping behaviour of GT–3% AT–MMT and GT–4% AT–MMT can also be analysed using the same method, and optimised extrusion pressure ranges are shown in Table 2.

3.3. Pressure optimisation by 3D printing checkerboard grid structure: Morphologies of 3D printed checkerboard grids with GT–AT–MMT bio-inks under predetermined pressure parameters are shown in Fig. 3. At lower printing pressures, the diameter of the extruded filament is very thin, and dragging deformation or intermittent connection occurs, which eventually leads to needle clogging and printing failure. At higher print pressures, the actual diameter of the extruded filament is much larger than the theoretical value, resulting in narrowing or merging filament spacing, especially in multi-layer printing, where a more evident material accumulation phenomenon occurs and ultimately leads to poor shape fidelity of the printing structure.

A needle with a diameter of 0.3 mm was used in the experiment. Thus, the theoretical diameter of the extruded filament was 0.30 mm. However, when the extruded cylindrical filament was deposited on the substrate, a certain degree of collapse would occur under the action of gravity because hydrogel is not a rigid material (Fig. 4*a*). Based on the printing experience parameters, the filament width is generally 1.25 times the theoretical diameter, which was 0.375 mm in this experiment. According to this width, the theoretical pore area can be obtained as $A_t = 0.39\ mm^2$. Then, for each 3D printed sample at a predetermined pressure, more than ten pores were selected and observed using a high-speed microscope camera, and the average pore area was taken as the actual pore area A_e (Fig. 4*b*). Finally, F_{ma} was calculated according to the formula and the statistical results are shown in Fig. 4*c*. The optimum printing pressure was obtained by combining the F_{ma} data results with the macro-printing effect analysis, as shown in Table 3. As the content of AT increases, the optimum pressure value increases possibly because AT increases the overall viscosity of the mixed bio-ink, which also corresponds to the characterisation results of subsequent mechanical properties.

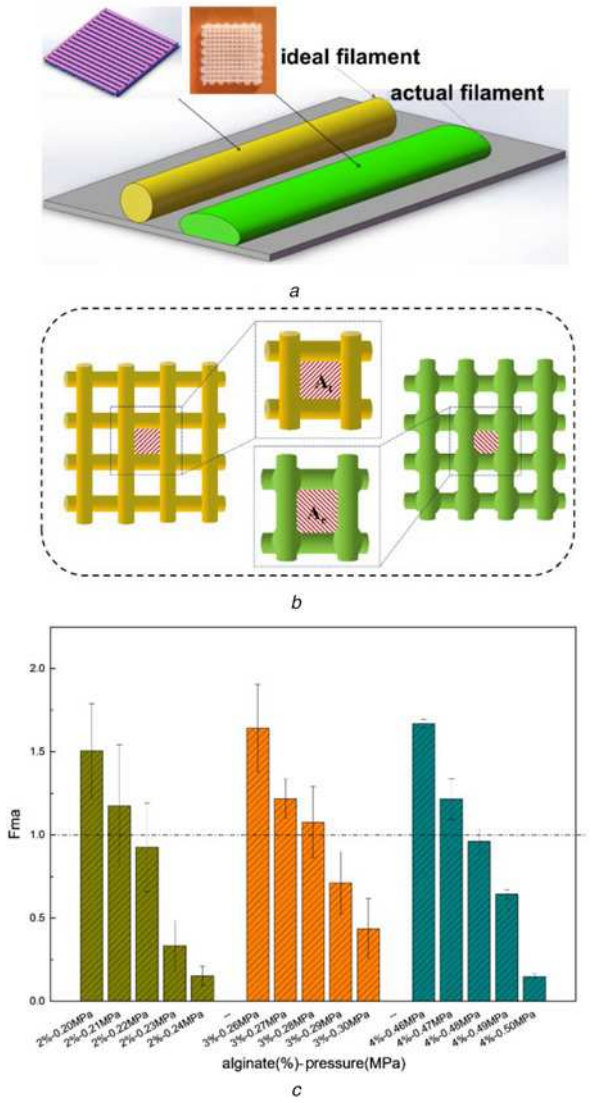

Fig. 4 *3D printing checkerboard grid model using variable concentrations of GT–AT–MMT bio-inks*
a Schematic diagram of theoretical filament morphology and actual filament morphology of 3D printing
b Schematic diagram of theoretical pore area A_t and actual pore area A_e of 3D printed checkerboard grid model
c Statistical results of F_{ma} measurement of GT–AT–MMT bio-inks at predetermined pressures

3.4. Tension test results and analysis: Fig. 5*a* shows the stress–strain curves of 3D printed GT–AT–MMT samples at various AT concentrations. Tensile strength and fracture strain of 3D printed samples increased with the increase of AT content, and the maximum tensile strength (0.467 MPa) of GT–4% AT–MMT sample was about eight times that of the GT–2% AT–MMT sample (0.058 MPa). The tension modulus (Fig. 5*b*) of 3D printed GT–AT–MMT samples was obtained from the linear region of the tensile stress–strain curves by the Origin software. The results reveal that the tension modulus of GT–AT–MMT is positively correlated with the crosslinking degree of the long chains in the hydrogel molecules. Under the immersion of sufficient

doi: 10.1049/mnl.2019.0712

Table 3 Optimal pressure for 3D printing variable GT–AT–MMT bio-inks

Bio-inks	GT–2% AT–MMT	GT–3% AT–MMT	GT–4% AT–MMT
optimal pressure	0.22 MPa	0.28 MPa	0.48 MPa

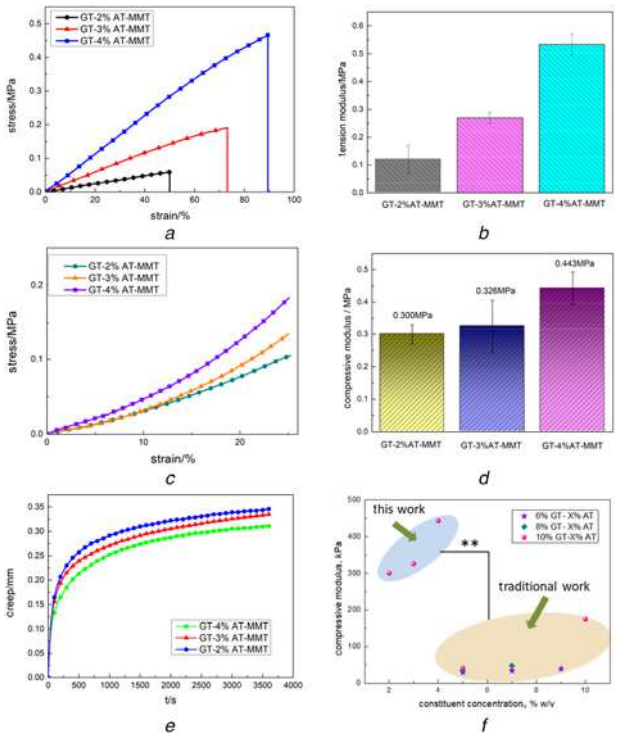

Fig. 5 *Characterisation of mechanical properties of 3D printed GT–AT–MMT samples*
a Tensile stress–strain curves
b Tension modulus of tensile test
c Compression stress–strain curves
d Compressive modulus of a compression test
e Creep deformation curves
f Comparison of compression modulus of 3D printed GT/AT-based hydrogels (**$P < 0.01$)

$CaCl_2$ solution, AT molecules in samples can be fully cross-linked, replacement reaction occurs between Ca^{2+} and Na^{+} in the AT molecular chains, and a Ca^{2+} connects two carboxyl groups (–COOH) to produce the connection effect, finally forming a network-like structure. The long-chain density in hydrogel increases and the number of cross-linked nodes increases significantly with the increase of AT content. Therefore, macroscopically, tensile strength and elastic modulus of hydrogel samples increase with the increase of AT concentration in GT–AT–MMT bio-inks.

3.5. Compression test results and analysis: The compressive stress–strain curves (Fig. 5*c*) of 3D printed GT–AT–MMT samples show that with the increase of AT content in the bio-inks, the additional stress is required for the sample to reach the same strain increases correspondingly. Taking the strain degree of 20% as an example, corresponding stresses of bio-inks with AT content of 2, 3, and 4% are 0.076, 0.092, and 0.126 MPa, respectively, which evidently increase with the increase of AT content. The compressive modulus (Fig. 5*d*) of 3D printed GT–AT–MMT samples was also obtained from the linear region of the tensile stress–strain curves by the Origin software. Fig. 5*d* shows that the compression modulus of the GT–4% AT–MMT sample is significantly higher than that of the GT–2% AT–MMT and GT–3% AT–MMT samples. This is mainly because the crosslinking density increases with the increase of AT content in hydrogel, and the cross-linked polymer network becomes tighter with the increase of strain. Therefore, the deformation resistance of hydrogel samples is significantly enhanced.

In this work, the compressive modulus of the GT–4% AT–MMT sample is as high as 0.443 MPa, which is clearly improved compared with previous research on mechanical properties of 3D printed samples using GT–AT as bio-inks (Fig. 5*f*). Di Giuseppe *et al.* [26] studied the print capability, print accuracy, and compressive behaviour of nine GT–AT components as 3D printing bio-inks. Uniaxial compression tests showed that the best component bio-ink (8% GT–7% AT) has a compressive modulus of 48.0 kPa. Shi *et al.* [27] used GT–AT as 3D printing bio-inks to prepare scaffolds for skin tissue engineering, and the uniaxial compression tests showed that Young's modulus of 10% GT–10% AT could reach 175.1 kPa. The comparison shows that the mechanical properties of GT–AT–MMT bio-ink in this work are significantly improved by adding MMT nanoparticles because the addition of MMT promotes the formation of hydrogen bonding force between GT–AT–MMT molecules. Thus the degree of crosslinking is improved, which is consistent with the above XRD and FTIR test results.

3.6. Creep test results and analysis: The creep curves (Fig. 5*e*) of 3D printed GT–AT–MMT samples show that the deformation degree in the initial stage increases rapidly. As the test progresses, the deformation rate gradually slows down, showing the trend of the second-stage creep characteristic curve mainly due to the existence of macroscopic grid structures and microscopic pore structures in the 3D printed GT–AT–MMT samples. In the early stage of the creep process, deformation resistance is very small such that the deformation rate is very large. The pores and macro grids inside the hydrogel are gradually filled, and resistance against deformation gradually increases with the increase of time such that the deformation rate decreases. When the same load (10 N) was applied, the minimum deformation (0.311 mm) occurred in the GT–4% AT–MMT sample with the highest AT content. This result is also attributed to the increase of the cross-linking degree caused by the increase of AT content, which makes the molecular network structure denser and enhances the creep deformation resistance of hydrogels.

4. Conclusions: In this study, a nanocomposite bio-ink for 3D printing was developed using a mixture of GT, AT, and nano-MMT. The 3D printing pressure of GT–AT–MMT bio-inks with variable AT contents was optimised by the extruding drop test and the experiment of 3D printing checkerboard grid structures. In addition, the mechanical properties of 3D printed GT–AT–MMT samples were studied by tensile, compression, and creep tests. The results showed that tensile strength and compressive strength increase, and creep deformation resistance enhances with the increase of AT content. In summary, the GT–AT–MMT nanocomposite hydrogel with good printing capability and excellent mechanical strength is expected to become an ideal 3D printing bio-ink for cartilage tissue engineering and regenerative medicine.

5 References

[1] Lin Z., Wu M., He H., *ET AL.*: '3D printing of mechanically stable calcium-free alginate-based scaffolds with tunable surface charge to

enable cell adhesion and facile biofunctionalization', *Adv. Funct. Mater.*, 2019, **29**, (9), p. 1808439
[2] Liu H., Zhou H., Lan H., *ET AL.*: '3D printing of artificial blood vessel: study on multi-parameter optimization design for vascular molding effect in alginate and gelatin', *Micromachines*, 2017, **8**, (8), p. 237
[3] Luo Y., Lin X., Huang P.: '3D bioprinting of artificial tissues: construction of biomimetic microstructures', *Macromol. Biosci.*, 2018, **18**, (6), p. 1800034
[4] Luo Y., Wei X., Huang P.: '3D bioprinting of hydrogel-based biomimetic microenvironments', *J. Biomed. Mater. Res. B, Appl. Biomater.*, 2019, **107**, (5), pp. 1695–1705
[5] Choi D.J., Park S.J., Gu B.K., *ET AL.*: 'Effect of the pore size in a 3D bioprinted gelatin scaffold on fibroblast proliferation', *J. Ind. Eng. Chem.*, 2018, **67**, pp. 388–395
[6] Wu Y., Lin Z.Y.W., Wenger A.C., *ET AL.*: '3D bioprinting of liver-mimetic construct with alginate/cellulose nanocrystal hybrid bioink', *Bioprinting*, 2018, **9**, pp. 1–6
[7] Hewes S., Wong A.D., Searson P.C.: 'Bioprinting microvessels using an inkjet printer', *Bioprinting*, 2017, **7**, pp. 14–18
[8] Freeman S., Ramos R., Chando P.A., *ET AL.*: 'A bioink blend for rotary 3D bioprinting tissue engineered small-diameter vascular constructs', *Acta Biomater.*, 2019, **95**, pp. 152–164
[9] Panda B., Mohamed N., Ahamed N., *ET AL.*: 'The effect of material fresh properties and process parameters on buildability and interlayer adhesion of 3D printed concrete', *Materials*, 2019, **12**, (13), p. 2149
[10] Yang X., Lu Z., Wu H., *ET AL.*: 'Collagen-alginate as bioink for three-dimensional (3D) cell printing based cartilage tissue engineering', *Mater. Sci. Eng. C*, 2018, **83**, pp. 195–201
[11] Compaan A.M., Christensen K., Huang Y.: 'Inkjet bioprinting of 3D silk fibroin cellular constructs using sacrificial alginate', *ACS Biomater. Sci. Eng.*, 2016, **3**, (8), pp. 1519–1526
[12] Markstedt K., Mantas A., Tournier I., *ET AL.*: '3D bioprinting human chondrocytes with nanocellulose–alginate bioink for cartilage tissue engineering applications', *Biomacromolecules*, 2015, **16**, (5), pp. 1489–1496
[13] Apelgren P., Karabulut E., Amoroso M., *ET AL.*: 'In vivo human cartilage formation in three-dimensional bioprinted constructs with a novel bacterial nanocellulose bioink', *ACS. Biomater. Sci. Eng.*, 2019, **5**, (5), pp. 2482–2490
[14] Yu F., Han X., Zhang K., *ET AL.*: 'Evaluation of a polyvinyl alcohol-alginate based hydrogel for precise 3D bioprinting', *J. Biomed. Mater. Res. A*, 2018, **106**, (11), pp. 2944–2954
[15] Peak C.W., Stein J., Gold K.A., *ET AL.*: 'Nanoengineered colloidal inks for 3D bioprinting', *Langmuir*, 2017, **34**, (3), pp. 917–925
[16] Bociaga D., Bartniak M., Grabarczyk J., *ET AL.*: 'Sodium alginate/gelatine hydrogels for direct bioprinting—the effect of composition selection and applied solvents on the bioink properties', *Materials*, 2019, **12**, (17), p. 2669
[17] Schuurman W., Levett P.A., Pot M.W., *ET AL.*: 'Gelatin-methacrylamide hydrogels as potential biomaterials for fabrication of tissue-engineered cartilage constructs', *Macromol. Biosci.*, 2013, **13**, (5), pp. 551–561
[18] Jeon O., Lee Y.B., Hinton T.J., *ET AL.*: 'Cryopreserved cell-laden alginate microgel bioink for 3D bioprinting of living tissues', *Mater. Today Chem.*, 2019, **12**, pp. 61–70
[19] Sarker B., Rompf J., Silva R., *ET AL.*: 'Alginate-based hydrogels with improved adhesive properties for cell encapsulation', *Int. J. Biol. Macromol.*, 2015, **78**, pp. 72–78
[20] Nadernezhad A., Caliskan O.S., Topuz F., *ET AL.*: 'Nanocomposite bioinks based on agarose and 2D nanosilicates with tunable flow properties and bioactivity for 3D bioprinting', *ACS Appl. Bio Mater.*, 2019, **2**, (2), pp. 796–806
[21] Zhai X., Ruan C., Ma Y., *ET AL.*: '3D-bioprinted osteoblast-laden nanocomposite hydrogel constructs with induced micro-environments promote cell viability, differentiation, and osteogenesis both in vitro and in vivo', *Adv. Sci.*, 2018, **5**, (3), p. 1700550
[22] Roopavath U.K., Soni R., Mahanta U., *ET AL.*: '3D printable SiO_2 nanoparticle ink for patient specific bone regeneration', *RSC Adv.*, 2019, **9**, (41), pp. 23832–23842
[23] Banerjee S.L., Swift T., Hoskins R., *ET AL.*: 'A muscle mimetic polyelectrolyte–nanoclay organic–inorganic hybrid hydrogel: its self-healing, shape-memory and actuation properties', *J. Mater. Chem. B*, 2019, **7**, (9), pp. 1475–1493
[24] Olad A., Zebhi H., Salari D., *ET AL.*: 'A promising porous polymer-nanoclay hydrogel nanocomposite as water reservoir material: synthesis and kinetic study', *J. Porous Mater.*, 2018, **25**, (3), pp. 665–675
[25] Zhang Y., Liu Y., Liu J., *ET AL.*: 'Super water absorbency OMMT/PAA hydrogel materials with excellent mechanical properties', *RSC Adv.*, 2017, **7**, (24), pp. 14504–14510
[26] Di Giuseppe M., Law N., Webb B., *ET AL.*: 'Mechanical behaviour of alginate-gelatin hydrogels for 3D bioprinting', *J. Mech. Behav. Biomed. Mater.*, 2018, **79**, pp. 150–157
[27] Shi L., Xiong L., Hu Y., *ET AL.*: 'Three-dimensional printing alginate/gelatin scaffolds as dermal substitutes for skin tissue engineering', *Polym. Eng. Sci.*, 2018, **58**, (10), pp. 1782–1790

doi: 10.1049/mnl.2019.0712